Control carrier recombination of multi-scale textured black silicon surface for high performance solar cells

M. Hong, G. D. Yuan, Y. Peng, H. Y. Chen, Y. Zhang, Z. Q. Liu, J. X. Wang, B. Cai, Y. M. Zhu, Y. Chen, J. H. Liu , and J. M. Li

Control carrier recombination of multi-scale textured black silicon surface for high performance solar cells

M. Hong,[1] G. D. Yuan,[2,a)] Y. Peng,[1,a)] H. Y. Chen,[1] Y. Zhang,[2] Z. Q. Liu,[2] J. X. Wang,[2] B. Cai,[1] Y. M. Zhu,[1] Y. Chen,[2] J. H. Liu,[2] and J. M. Li[2]

[1]Shanghai Key Lab of Modern Optical System, Engineering Research Center of Optical Instrument and System, Ministry of Education, University of Shanghai for Science and Technology, Shanghai 200093, China
[2]Semiconductor Lighting R&D Center, Institute of Semiconductors, Chinese Academy of Sciences, Beijing 100083, China

We report an enhanced performance of multi-scale textured black silicon solar cell with power conversion efficiency of 15.5% by using anisotropic tetramethylammonium hydroxide etching to control the recombination. The multi-scale texture can effectively reduce the surface reflectance in a wide wavelength range, and both the surface and Auger recombination can be effectively suppressed by etching the samples after the n^{++} emitter formed. Our result shows that the reformed solar cell has higher conversion efficiency than that of conventional pyramid textured cell (15.3%). This work presents an effective method for improving the performance of nanostructured silicon solar cells. © 2014 AIP Publishing LLC. [http://dx.doi.org/10.1063/1.4884899]

Surface reflection is one of the main factors that limit the power conversion efficiency (CE) of solar cells. Reducing the surface reflection is an effective way to improve the performance of the photovoltaic cells. Micro-scale pyramid structure is widely used in industrial production,[1] which enhances light absorption by giving the reflected light a second chance to enter the solar cell,[2,3] but it has poor performance for high energy photons whose wavelength is from 400 to 500 nm due to the limit of geometric optics effect.[4] Quarter-wavelength-thick antireflection coating (ARC) is another method to suppress the surface reflection by destructing interference.[5–7] However, the ARC works only at an individual wavelength and, more important, the performance of ARC is limited by the incident angle.

In order to overcome such problems, silicon nanowires (SiNWs), made by metal assisted etching, have been widely adopted in single crystal silicon[3,8–21] and organic-silicon solar cell.[22,23] Since a gradient refractive index system is formed by the air-to-wire interface, the SiNWs can suppress Fresnel reflection over a broad wavelength range and various angles of incidence.[3,8] But, the length of SiNWs should be controlled in the range of 2–6 μm for achieving an extremely low reflectance,[10,21] which causes strong surface recombination due to the large surface area.[9,10] Additionally, during the process of n^+ emitter formed, the SiNWs itself changes into "dead layer" after the heavy phosphorus diffusion by changing the doping profile,[3,8,12] where the minority carrier lifetime is extremely low due to the serious Auger recombination suffered from the excessive doping. Moreover, the length reduction of SiNWs by controlling the fabricating conditions cannot suppress the Auger recombination effectively. Previous work[3] has reported the same textured solar cell with CE of 17.1%, but its internal quantum efficiency (IQE) at the short wavelength range of 400–500 nm is still poor, the reason is that the length of SiNWs is reduced

before phosphorous diffused so the Auger recombination is not effectively suppressed. If we use light doping to suppress Auger recombination,[12] the ohmic contact and the homogeneity of surface sheet resistance become the new problems. As a result, an effective method is needed to suppress the Auger recombination under the conditions of heavy phosphorus diffusion and then make the SiNWs solar cells more suitable for mass production.

In this work, in order to obtain a higher CE of nanostructure solar cells, we focus on suppressing the Auger recombination of multi-scale textured black silicon by a systematic etching process. The measurements of reflectance show that the multi-scale texture can greatly reduce the surface reflectance to ~4% while the length of SiNWs is only about 300 nm. Unlike the previous method for simply reducing the length of SiNWs, an anisotropic tetramethylammonium hydroxide (TMAH) solution is used to etch the samples after the heavy phosphorus diffusion. This process has two functions: first, it can suppress the surface recombination by reducing the length of SiNWs; second, it can suppress the Auger recombination by reducing the thickness of "dead layer." Then, the surface and Auger recombination can be suppressed effectively at the same time. Furthermore, the results of carrier lifetime of etched samples by TMAH show that, under the same TMAH etching time, the minority carrier lifetime of samples, which are etched at first and then diffused by phosphorus, is higher than that of the samples which are phosphorus diffused at first and then etched. It indicates that our method can not only suppress the surface recombination effectively but also suppress the Auger recombination, which leads to improvement of the IQE, short-circuit current density (J_{sc}), and open–circuit voltage (V_{oc}). Our best solar cell demonstrates a CE of 15.5%, which has an increase of 3.3% than that without TMAH etching (12.2%) and higher than that of traditional pyramid textured solar cell (15.3%).

In the experiments, solar-grade, 180 μm-thick, boron-doped p-type c-Si (100) wafers with a resistivity of 1.6 Ω cm

a)Authors to whom correspondence should be addressed: Electronic addresses: gdyuan@semi.ac.cn and py@usst.edu.cn.

and a minority carrier lifetime (τ) in range of 20–25 μs were used. The wafers were divided into two groups: group A as experimental samples used for solar cells fabricating; group B as reference samples used only for minority lifetime testing. Each wafer of groups A and B was cut into square of 4.5×4.5 cm^2 and immersed in the solution of 20 wt. % NaOH for 10 min at 80 °C to remove the saw damage, followed by a standard RCA cleaning. After that, the pyramid structure was fabricated in the solution of 2 wt. % NaOH, 2 wt. % Na$_2$SiO$_3$, and 5 vol. % isopropyl alcohol (IPA) for 30 min at 75 °C. Then the SiNWs were fabricated by two-step metal-assisted chemical etching as follows: first, the silver particles were uniformly deposited on the silicon wafers in a mixed solution of 1 mM AgNO$_3$ and 0.5 vol. % HF for 90 s at room temperature, then immersed in a mixed solution of 3 vol. % H$_2$O$_2$ and 12.5 vol. % HF for 20 s at room temperature. After the SiNWs fabricating, the wafers were treated with a concentrated HNO$_3$ solution for 2 h to remove the residual Ag particles. Then, the multi-scale textured black silicon wafers were dipped into a buffered oxide etch (BOE) solution to remove the oxide and then rinsed with deionized water. The multi-scale structure was fabricated on both sides of silicon wafer. Finally, we used 1 vol. % TMAH solution to etch the reference samples of group B for varied time (10–50 s).

For solar cells fabrication, the n^{++} emitter was formed with a liquid POCl$_3$ diffusion on the front surfaces of both groups of wafers, and the backsides were protected by SiO$_2$ grown by plasma-enhanced chemical vapor deposition (PECVD). After removing the phosphor-silicate-glass (PSG) on the front surface and SiO$_2$ on backside by BOE, we used 1 vol. % TMAH solution to etch the experimental samples of group A for varied time (10–50 s). Afterward, the aluminum back-surface-field (Al-BSF) was formed by the conventional screen-print technique. Front grids consist of Ti/Ag (200 nm/2500 nm) were fabricated by the E-beam evaporating through a metal mask designed as 1×1 cm^2, and back metal contact was made by evaporating Al/Ag (1000 nm/500 nm). Finally, each wafer was cut into 9 cells with the area of 1×1 cm^2, and an 80 nm-thick SiN$_x$ passivation layer was deposited by PECVD. Several standard pyramid structure solar cells were added for comparison. Surface morphologies were examined by a scanning electron microscope (SEM).

Reflectance spectra were measured by a fiber spectrometer equipped with an integrating sphere. Solar cell performance was obtained under a standard 1-sun illumination with a simulator and a source meter. Effective carrier lifetime was tested using a lifetime tester (WT2000), and external quantum efficiency (EQE) of cells was measured by a quantum efficiency tester (Solar Cell Scan 100).

Figure 1(a) shows the surface morphology of textured silicon after the SiNWs were formed. The pyramid structure with diameter of 3–5 μm is covered by the SiNWs with length of about 300 nm, whose density decreases gradually from the bottom to top. Besides, the SiNWs are vertical to the surface of pyramid with $\langle 111 \rangle$ oriented, this characteristic can provide better controllability for the TMAH etching. Because the TMAH solution has an excellent anisotropic etching characteristic, that the etching rate of (111) plane is 10 μm/h, and the etching rate ratio between (111) and (100) plane is about 0.04 which is much higher than other anisotropic alkaline solution for single crystal silicon (NaOH, KOH, etc.).[24,25]

Based on the multi-scale texture fabricated above, we performed a TMAH etching after the phosphorus diffusion. The different evolutions of surface morphology under TMAH etching time of 10 s, 20 s, 30 s, 40 s, and 50 s are shown in Figs. 1(b)–1(f). It is clear that the length and density of SiNWs continuously decrease with the etching time prolongs, but the size of pyramid structure is not obviously changed. This is caused by that the TMAH etching process combines a low etching rate on (111) plane and a high anisotropic etching ratio of (111)/(100), so it does not damage the surface of pyramid during the TMAH etching process. When the etching time reaches 50 s, most of the SiNWs have been removed, only a little is remained on the bottom of pyramid.

To characterize the antireflection characteristic of multi-scale textured black silicon, reflectance of samples under varied TMAH etching time are measured in the wavelength range of 400–1100 nm. Figure 2 shows the reflectance spectra of multi-scale textured black silicon under different TMAH etching time varies from 0 to 50 s. The average reflectance is about 4% before TMAH etching, which indicates that the multi-scale texture can effectively suppresses the reflection in whole spectrum, especially at the short wavelength range of 400–500 nm. This is because the density of
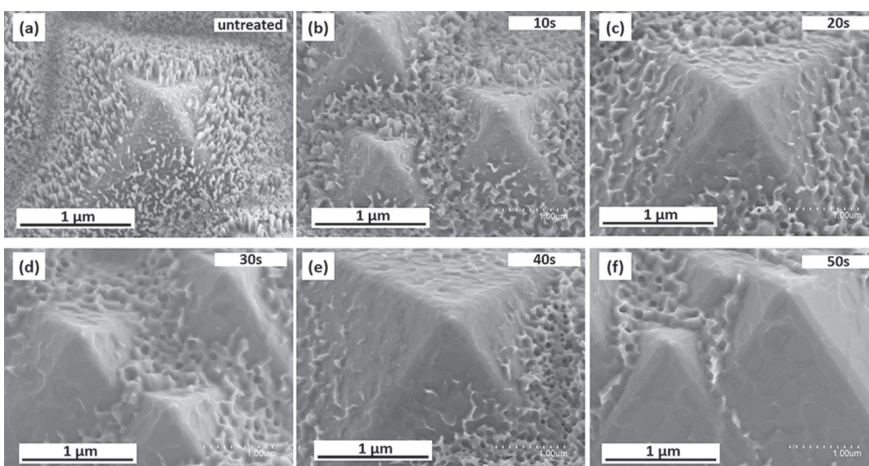
FIG. 1. SEM images of multi-scale textured black silicon surface morphology under different etching time of TMAH-based solution: (a) untreated, (b) 10 s, (c) 20 s, (d) 30 s, (e) 40 s, and (f) 50 s. Each SEM images is taken at a 25° angle to the surface.
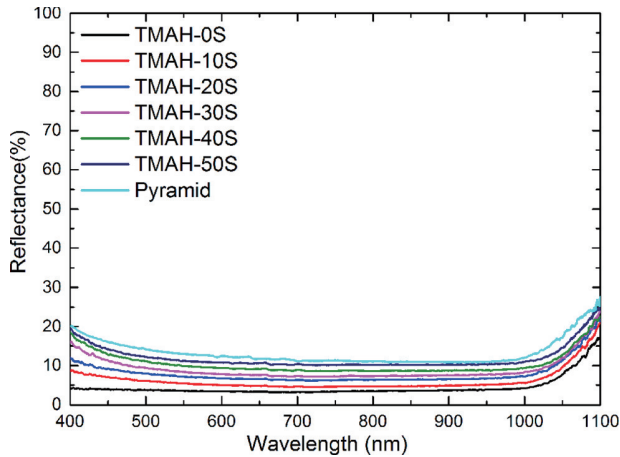
FIG. 2. Reflectance spectra of multi-scale textured black silicon under different TMAH etching time, and the spectrum of standard pyramid structure surface is also shown for comparison.

the SiNWs increases gradually from top to bottom of the pyramid, i.e., the graded-index refraction is formed along the pyramid structure, which makes the multi-scale structure working as an optical buffer. As a result, the multi-scale structure can reduce the great mismatch in effective refractive index between a silicon substrate ($n \approx 3.85$) and the air ($n \approx 1$). Then, as the etching time increases, the reflectance increases gradually which is caused by the decrease of the length and density of SiNWs. When the etching time prolonged to 50 s, the average reflectance reaches 12%, which is still lower than that of pyramid structure with average reflectance of 14%, but the gap is small. Based on this result, we conclude that the reflectance maybe higher than that of pyramid structure if we continue prolonging the etching time, that should decrease the J_{sc} and CE.

To verify the effect of TMAH etching on improving the collection ability of photon-generated carriers, we measured the spectral dependence of EQE. Figure 3 shows the IQE spectra derived from EQE as $IQE = EQE/(1 - R)$, where R stands the reflectance. The IQE of the cell before TMAH etching is low, indicating a high recombination rate. Especially, the IQE in 400–500 nm range is extremely poor
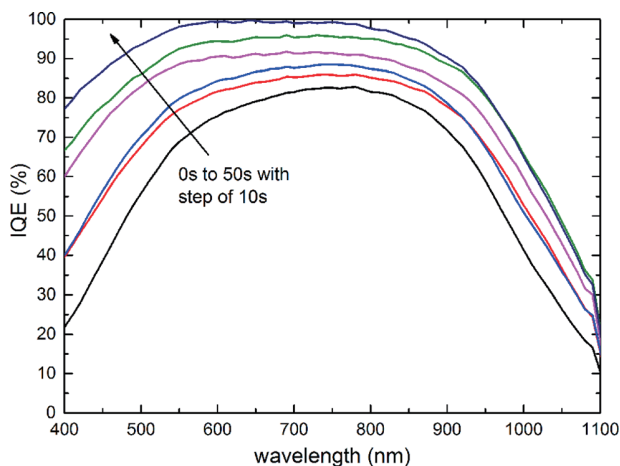
FIG. 3. IQE of multi-scale textured black silicon solar cells under different TMAH etching time.

($\sim$20%), which is actually caused by the serious Auger recombination. Normally, the poor blue spectra response exists in most nanostructured silicon solar cells, which limits the J_{sc} and CE. It is clear that the IQE increases with the prolonging of TMAH etching time, which is caused by the effective suppression of Auger recombination. Correspondingly, the back side has the same structure as that of front side, so the photovoltaic response in long wavelength range (900–1100 nm) has also been improved due to the suppressed surface recombination.

To prove the effect of our method on the suppressing of Auger recombination, we measured the minority carrier lifetime. Figures 4(a$_1$)–4(a$_5$) show lifetime mappings of group A under the TMAH etching time from 10 s to 50 s, respectively. We can see that with the increase of TMAH etching time, the color of mappings gradually turns into blue/dark from red, which indicates an improvement of minority carrier lifetime (3.14 μs, 3.28 μs, 5.15 μs, 7.14 μs, and 8.95 μs, respectively). Figures 4(b$_1$)–4(b$_5$) show lifetime mappings of group B under the TMAH etching time from 10 s to 50 s, respectively. The sustained increasing of minority carrier lifetime (2.77 μs, 2.86 μs, 3.11 μs, 3.74 μs, and 6.23 μs, respectively) due to the suppression of surface recombination. Importantly, the lifetime of group B is lower than that of group A under the same TMAH etching time. Because the samples of groups A and B have the same length of SiNWs (i.e., the same surface recombination) under the same TMAH etching time, we can conclude that the further improvement of minority carrier lifetime comes from the suppression of Auger recombination due to the reduction of thickness of "dead layer." This result demonstrates that our method is more effective for suppressing both the surface and Auger recombination than simply reducing the length of SiNWs before phosphorus diffusion.

After ohmic contacting and surface passivation, we investigated the output CE performances of our cells. Figure 5 presents J–V curves of typical solar cells under different TMAH etching time for qualitative comparison. Table I summarizes the V_{oc}, J_{sc}, Fill Factor (FF), and CE of the solar cells, and the cell of standard pyramid structure is added for comparison. We can see that the cell without TMAH etching has a low V_{oc} (556 mV) and J_{sc} (29.1 mA/cm^2), which is due to the poor carrier collection ability associated with the serious surface and Auger recombination. After the TMAH etching, the cells have a gradually increased J_{sc} (as shown in Table I) due to the improved collection ability of photo-generated carriers (Fig. 5). And the suppressed surface and Auger recombination can reduce the dark saturation current density (J_0) of multi-scale textured solar cells. According to Eq. (1) in Ref. 13, V_{oc} is a function of J_0 and J_{sc}

$$V_{oc} = \frac{k_B T}{q} \ln\left(1 + \frac{J_{sc}}{J_0}\right), \tag{1}$$

where k_B is Boltzmann's constant, T is temperature, q is the charge of an electron, and J_{sc} is the short circuit current density. So the V_{oc} has an analogous increasing trend (as shown in Table I) with J_{sc}. When the etching time increases to 50 s, we get the best cell with CE of 15.5% among those samples of multi-scale textured solar cells (average CE is 15.2%
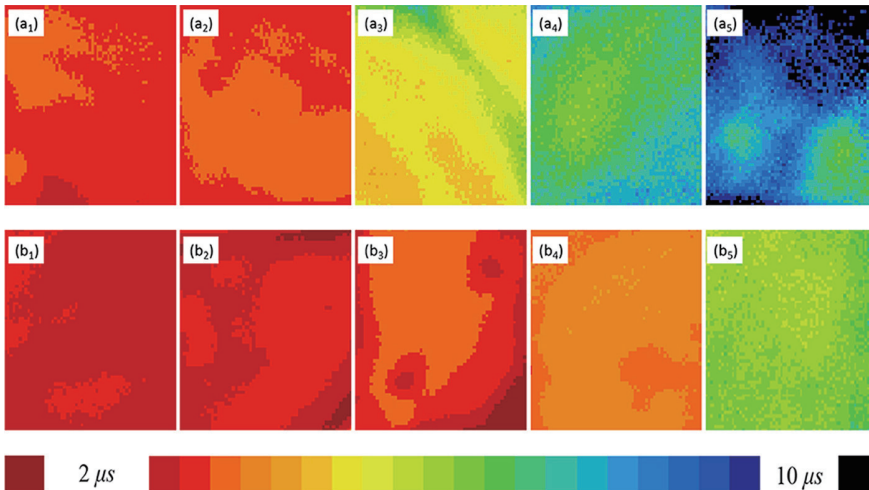
FIG. 4. Minority carrier lifetime evolution of black silicon under different TMAH etching time: (a_1)–(a_5) are the lifetime mappings of group A (10 s–50 s with interval 10 s, respectively); (b_1)–(b_5) are the lifetime mappings of group B (10 s–50 s with interval 10 s, respectively).

TABLE I. Photovoltaic characteristics of multi-scale textured black silicon solar cells under different TMAH time, and pyramid texture is listed for comparison.

Samples	V_{oc} (mV)	J_{sc} (mA/cm^2)	FF (%)	CE (%)
TMAH etching 0 s cell	556	29.1	74.1	12.2
TMAH etching 10 s cell	561	30.8	71.9	12.8
TMAH etching 20 s cell	577	31.7	75.8	13.9
TMAH etching 30 s cell	579	34.0	71.8	14.4
TMAH etching 40 s cell	581	34.9	72.3	15.1
TMAH etching 50 s cell	584	35.9	74.0	15.5
Pyramid structure cell	599	34.2	74.8	15.3
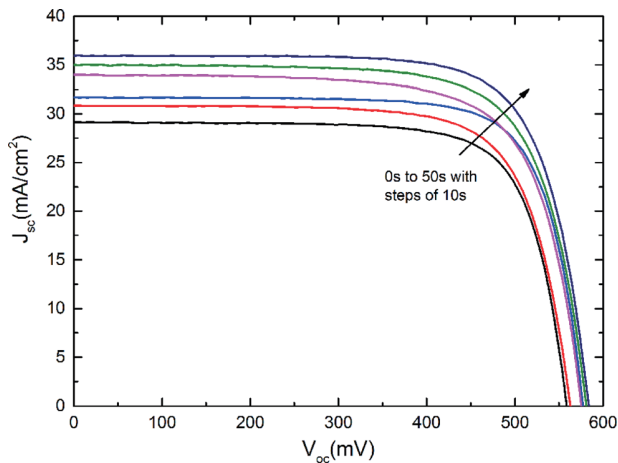
FIG. 5. J-V characteristics of multi-scale textured black silicon solar cells under different TMAH etching time.

evaluated from 9 cells), and it is higher than that of pyramid textured cell with CE of 15.3% (average CE is 14.9% evaluated from 9 cells) due to the higher J_{sc} caused by the enhanced photon capturing ability of multi-scale structure. However, the V_{oc} is still lower than that of pyramid textured cell, this is probably result from the worse passivation performance of SiN$_x$ layer for nanostructured surface than that for smooth surface (the sidewall of pyramid texture).[26]

In summary, we experimentally fabricated a multi-scale textured black silicon by combining a graded density SiNWs and micron-scale pyramid structure, which shows an excellent

antireflection ability. By utilizing the anisotropic-etching TMAH solution to treat the samples after heavy phosphorus diffusion, both the surface and Auger recombination can be suppressed effectively at the same time, leading to an obvious increase of V_{oc} and J_{sc}. With the recombination suppressed multi-scale textured black silicon, the solar cell obtains an excellent CE of 15.5%, which is higher than that of the cell without TMAH etching (12.2%) and the traditional micro-scale pyramid textured solar cell (15.3%). These results can be utilized to effectively improve the performance of nanostructured silicon solar cells, which can also be easily applied to mass-production.

[1]P. K. Basu, D. Sarangi, K. D. Shetty, and M. B. Boreland, Sol. Energy Mater. Sol. Cells **113**, 37–43 (2013).
[2]H.-P. Wang, T.-Y. Lin, C.-W. Hsu, M.-L. Tsai, C.-H. Huang, W.-R. Wei, M.-Y. Huang, Y.-J. Chien, P.-C. Yang, C.-W. Liu, L.-J. Chou, and J.-H. He, ACS Nano **7**(10), 9325–9335 (2013).
[3]F. Toor, H. M. Branz, M. R. Page, K. M. Jones, and H.-C. Yuan, Appl. Phys. Lett. **99**(10), 103501 (2011).
[4]R. B. Stephens and G. D. Cody, Thin Solid Films **45**(1), 19–29 (1977).
[5]S. L. Diedenhofen, G. Vecchi, R. E. Algra, A. Hartsuiker, O. L. Muskens, G. Immink, E. P. A. M. Bakkers, W. L. Vos, and J. G. Rivas, Adv. Mater. **21**(9), 973–978 (2009).
[6]Z. Ge, P. Rajbhandari, J. Hu, A. Emrani, T. P. Dhakal, C. Westgate, and D. Klotzkin, Appl. Phys. Lett. **104**(10), 101104 (2014).
[7]N. Sahouane and A. Zerga, Energy Procedia **44**, 118–125 (2014).
[8]H.-C. Yuan, V. E. Yost, M. R. Page, P. Stradins, D. L. Meier, and H. M. Branz, Appl. Phys. Lett. **95**(12), 123501 (2009).
[9]D. Kumar, S. K. Srivastava, P. K. Singh, M. Husain, and V. Kumar, Sol. Energy Mater. Sol. Cells **95**(1), 215–218 (2011).
[10]H. Li, R. Jia, C. Chen, Z. Xing, W. Ding, Y. Meng, D. Wu, X. Liu, and T. Ye, Appl. Phys. Lett. **98**(15), 151116 (2011).
[11]X. Li and P. W. Bohn, Appl. Phys. Lett. **77**(16), 2572 (2000).
[12]J. Oh, H. C. Yuan, and H. M. Branz, Nat. Nanotechnol. **7**(11), 743–748 (2012).
[13]Y. Qi, Z. Wang, M. Zhang, F. Yang, and X. Wang, J. Phys. Chem. C **117**(47), 25090–25096 (2013).

[14]J. Yeom, D. Ratchford, C. R. Field, T. H. Brintlinger, and P. E. Pehrsson, Adv. Funct. Mater. **24**(1), 106–116 (2014).

[15]G. Yuan, R. Mitdank, A. Mogilatenko, and S. F. Fischer, J. Phys. Chem. C **116**(25), 13767–13773 (2012).

[16]G. D. Yuan, Y. B. Zhou, C. S. Guo, W. J. Zhang, Y. B. Tang, Y. Q. Li, Z. H. Chen, Z. B. He, X. J. Zhang, P. F. Wang, I. Bello, R. Q. Zhang, C. S. Lee, and S. T. Lee, ACS Nano **4**(6), 3045–3052 (2010).

[17]G. D. Yuan, T. W. Ng, Y. B. Zhou, F. Wang, W. J. Zhang, Y. B. Tang, H. B. Wang, L. B. Luo, P. F. Wang, I. Bello, C. S. Lee, and S. T. Lee, Appl. Phys. Lett. **97**(15), 153126 (2010).

[18]C. S. Guo, L. B. Luo, G. D. Yuan, X. B. Yang, R. Q. Zhang, W. J. Zhang, and S. T. Lee, Angew. Chem. **48**(52), 9896–9900 (2009).

[19]J. Jie, W. Zhang, K. Peng, G. Yuan, C. S. Lee, and S.-T. Lee, Adv. Funct. Mater. **18**(20), 3251–3257 (2008).

[20]L. Liu, K. Q. Peng, Y. Hu, X. L. Wu, and S. T. Lee, Adv. Mater. **26**(9), 1410–1413 (2014).

[21]J.-Y. Jung, H.-D. Um, S.-W. Jee, K.-T. Park, J. H. Bang, and J.-H. Lee, Sol. Energy Mater. Sol. Cells **112**, 84–90 (2013).

[22]F. Zhang, B. Sun, T. Song, X. Zhu, and S. Lee, Chem. Mater. **23**(8), 2084–2090 (2011).

[23]X. Shen, B. Sun, D. Liu, and S. T. Lee, J. Am. Chem. Soc. **133**(48), 19408–19415 (2011).

[24]J. S. You, D. Kim, J. Y. Huh, H. J. Park, J. J. Pak, and C. S. Kang, Sol. Energy Mater. Sol. Cells **66**(1–4), 37–44 (2001).

[25]A. Merlos, M. Acero, M. H. Bao, J. Bausells, and J. Esteve, Sens. Actuators, A **37–38**, 737–743 (1993).

[26]Z. Zuo, K. Zhu, G. Cui, W. Huang, J. Qu, Y. Shi, Y. Liu, and G. Ji, Sol. Energy Mater. Sol. Cells **125**, 248–252 (2014).